CrossMark

Dynamic Recrystallization Kinetics and Microstructural Evolution for LZ50 Steel During Hot Deformation

Shiwen Du, Shuangmei Chen, and Jianjun Song

The dynamic recrystallization (DRX) behavior of LZ50 steel was investigated using hot compression tests at a deformation temperature of 870-1170 °C and a strain rate of 0.05-3 s^{-1}. The effects of deformation temperature, strain, strain rate, and initial austenite grain size on the microstructural evolution during DRX were studied in detail. The austenite grain size of DRX was refined with increasing strain rate and decreasing temperature, whereas the initial grain size had no influence on DRX grain size. A model based on the Avrami equation was proposed to estimate the kinetics of the DRX under different deformation conditions. A DRX map, which was derived from the DRX kinetics, the recrystallized microstructure, and the flow stress analysis, can be used to identify optimal deformation conditions. The initiation of DRX was lower than Z_c (critical Zener-Hollomon parameter) and higher than ε_c (critical strain). The relationship between the DRX microstructure and the Z parameter was analyzed. Fine DRX grain sizes can be achieved with a moderate Z value, which can be used to identify suitable deformation parameters.

1. Introduction

Dynamic recrystallization (DRX) is the most dominant restoration mechanism during hot deformation, and it affects the final microstructure and mechanical properties of deformed materials (Ref 1-3). The ability to predict the DRX kinetics and grain size in different hot deformation regimes is a prerequisite for designing certain industrial processes. Considerable research has been focused on modeling DRX behavior (Ref 4-6). DRX characteristics and grain size have been studied in detail experimentally and theoretically (Ref 7-9). However, DRX behavior and microstructure evolution in LZ50 steel have not been investigated. LZ50 is one kind of representative medium carbon steel and is used widely in railway components. To refine the grains and to improve the mechanical properties of LZ50 through hot deformation, the DRX kinetics and microstructural evolution of LZ50 should be investigated.

Microstructural evolution during the hot deformation of different materials is complex, and it is affected by different parameters such as temperature, strain, strain rate, and initial grain size (Ref 10-12). In this study, the effect of thermomechanical parameters, including strain rate, strain, initial grain size, and temperature on the DRX microstructure has been investigated. A model based on the Avrami equation has been developed to estimate DRX kinetics. Proper selection of deformation parameters such as temperature and strain rate is

essential to obtain an appropriate microstructure (Ref 13). Based on the DRX principles, a DRX map is plotted, which will provide guidelines for selecting suitable deformation parameters.

2. Experimental Procedures

LZ50 steel was used in this investigation. Its chemical composition is listed in Table 1. Cylindrical compression samples (15 mm high, 10 mm diameter) were prepared from an as-received square blank. Their initial grain microstructure is shown in Fig. 1(a). The grain size distribution is shown in Fig. 1(b). Hot compression tests were performed using a Gleeble-3500 thermomechanical simulator. Graphite lubricant was used to fill in the grooves and was applied to the sample end faces to reduce friction. All compression samples were austenitized at 1200 °C for 5 min (5 °C/s) and then cooled (5 °C/s) to the hot compression testing temperatures that ranged from 870 to 1170 °C. After holding at the deformation temperature for 30 s to eliminate the thermal gradient, samples were deformed to a true strain of 0.912 at strain rates of 0.05-3 s^{-1}. Samples were water quenched within 30 s after deformation to preserve the austenite microstructure. Different reheating schedules were used to study the effect of initial austenite grain size on microstructural evolution during DRX. Specimens were heated to 970, 1020, 1070, and 1170 °C and held for 5 min to obtain different initial austenitic grain sizes. Subsequently, specimens were cooled at 5 °C/s to a deformation temperature of 950 °C, held for 30 s to stabilize the temperature, compressed to a prescribed strain of 0.912 at a constant true strain rate of 0.5 s^{-1}, and quenched with water. All deformed samples were sectioned along the longitudinal compression axis, polished, and etched chemically with a saturated aqueous picric acid solution to study the microstructure. The austenite recrystallization grain size was measured on samples taken from their central region by the "linear intercept" procedure using an optical microscope. MIAPS

Shiwen Du, Shuangmei Chen, and Jianjun Song, School of Materials Science and Technology, Taiyuan University of Science and Technology, Shanxi Key Laboratory of Metal Forming Theory and Technology, Taiyuan, Shanxi, China. Contact e-mail: tykddsw@126.com.

Table 1 Chemical composition of the LZ50 steel (in wt.%)

C	Mn	Si	P	S	Cr	Ni	Cu	Al	V	N
0.51	0.74	0.29	0.008	0.002	0.013	0.008	0.006	0.02	0.02	0.0034
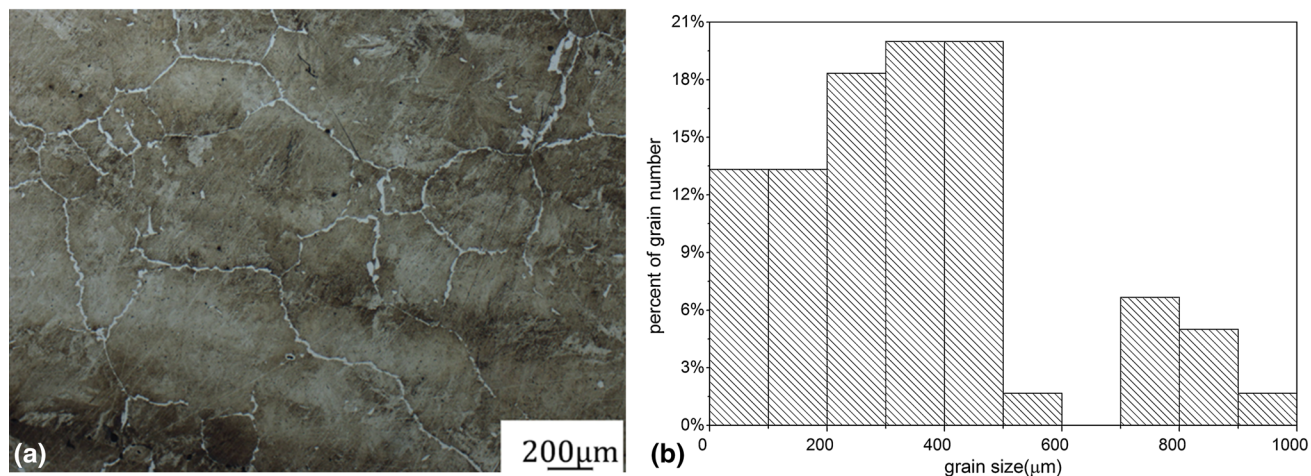
Fig. 1 Microstructure and grain size distribution of initial LZ50: (a) microstructure of initial LZ50 and (b) grain size distribution

software was used when measuring the grain size by the intercept method. First, a suitable magnification was chosen. For each of the five sample views chosen, and using MIAPS, 5×5 grid measuring lines were used. The average grain size was measured per view. These results were averaged to obtain a total average grain size.

3. Effect of Deformation Parameters on DRX Microstructure

3.1 Effect of Deformation Temperature

The effect of deformation temperature on microstructural evolution during DRX in LZ50 steel was investigated at a strain of 0.912 and a strain rate of 0.1 s^{-1}. Figure 2 shows the optical deformed microstructures at the different deformation temperatures. The average grain sizes were 18.80, 30.12, 40.39, 62.57, and 180.19 μm, at 870, 970, 1020, 1070, and 1170 °C, respectively. At 870 °C, the original grains were elongated along the deformation direction, and many new fine DRX grains emerged at prior grain boundaries. A necklace structure had formed, which demonstrates the occurrence of DRX. As the deformation temperature increased to 970 °C, equiaxed grains were visible. The original grains were replaced by new fine DRX grains, and the DRX process was completed. Flow stress remained constant during the steady-state deformation. As the deformation temperature increased to 1020 °C, the DRX grain size increased with increase in deformation temperature. As the deformation temperature increased to 1070 °C, the DRX grains coarsened noticeably compared with the behavior at 970 °C. At 1170 °C the DRX grains coarsened significantly compared with those at 1020 °C. Therefore, the austenite grain size increased with increase in deformation temperature. This occurs mainly because the deformation stored energy and the DRX nucleation rate increase with increase in deformation

temperature. A higher deformation temperature yields a more rapid grain boundary migration.

3.2 Effect of Strain Rate

Figure 3 shows the microstructural evolution of LZ50 steel that is deformed to a strain of 0.912 at 1020 °C with different strain rates. All microstructures were characterized by equiaxed grains, which indicates that complete DRX had occurred. In Fig. 3, the average grain sizes are 44.81, 40.39, 38.26, 34.2, and 24.61 μm for strain rates of 0.05, 0.1, 0.5, 1, and 3 s^{-1}, respectively. The grain size decreased with increase in strain rate from 0.05 to 3 s^{-1}. In general, an increase in strain rate will increase the deformation stored energy, and the dislocation density and grain nucleation sites increase simultaneously. An increased number of substructures will be generated in the original grains. A higher strain rate will reduce the DRX time. There is insufficient time for grains to grow at a high strain rate, because of the short recrystallization time.

3.3 Effect of Strain

Figure 4 shows the LZ50 steel microstructures that are deformed to different strains with a strain rate of 0.5 s^{-1} and a deformation temperature of 1070 °C. Average grain sizes were measured as 102.85, 101.31, 95.92, 54.02, and 48.63 μm. Figure 4(a) shows that the initial austenite grain shapes were elongated after being deformed to a strain of 0.163, and some bulging of grain boundaries was visible. Figure 4(b) shows that small new grains formed along the original boundaries. As the strain increased, significantly more new small grains nucleated at pre-existing grain boundaries. At a strain of 0.912, recrystallized grains covered the entire microstructure and appeared nearly equiaxed, which indicates that complete DRX was achieved. For isothermal constant strain rate compression, with a deformation temperature of 1070 °C and a strain rate of 0.5 s^{-1}, the critical strain (ε_c), peak strain (ε_p), and steady-state
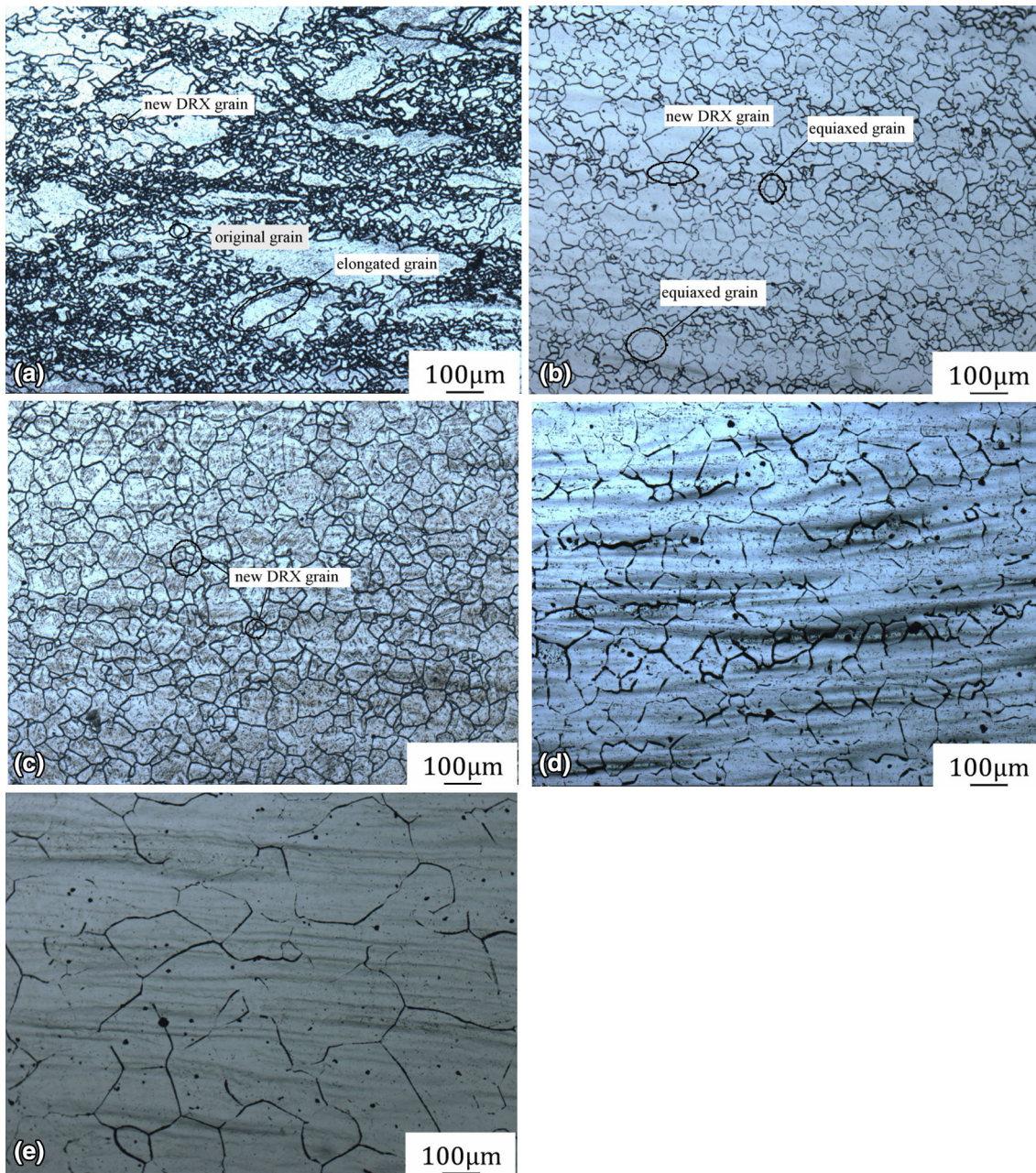
Fig. 2 Optical deformed microstructures at different temperatures ($\varepsilon = 0.912$, $\dot{\varepsilon} = 0.1\ \mathrm{s}^{-1}$): (a) 870 °C; (b) 970 °C; (c) 1020 °C; (d) 1070 °C; and (e) 1170 °C

strain (ε_{ss}) were 0.182, 0.353, and 0.681, respectively. The relationship between flow stress, recrystallized fraction, and strain is shown in Fig. 5.

The recrystallized grain sizes are likely to be determined by the balance between the growth (G) and nucleation rate (N). Steady-state grain sizes can be expressed as being proportional to $(G/N)^{1/3}$, according to Derby and Ashby's model of dynamically recrystallized grain size (Ref 14). The nucleation rate N is expected to increase exponentially with strain, but the growth rate G will increase mildly with strain. The recrystallized grain sizes are expected to depend on the strain and to decrease with an increase in deformation strain.

Figure 5 shows that the strain had an important effect on DRX. The strain relationship was $\varepsilon_{(a)} < \varepsilon_c < \varepsilon_{(b)} < \varepsilon_{(c)} < \varepsilon_p < \varepsilon_{(d)} < \varepsilon_{ss} < \varepsilon_{(e)}$. In Fig. 4(a), the strain was less than the

critical strain of DRX and the DRX fraction was 0. The grain was only elongated. Grain elongation and boundary serration increased with increase in strain. In Fig. 4(b) and (c), strain existed between the critical and peak strains, and the DRX fraction was less than 5%. New DRX grains formed on the serrated grain boundaries and DRX was initiated. In Fig. 4(d), strain existed between the peak and steady-state strains, and the DRX fraction approximated 50%. Many new DRX grains covered the previous grain boundaries and the first layer of a necklace structure started to form around the original boundaries. DRX occurred noticeably, and the grain size decreased rapidly. In Fig. 4(e), the strain was greater than the steady-state strain, and the DRX process was complete. The initiation of DRX requires that the strain reaches or exceeds the critical strain. When the strain is less than the critical strain, work
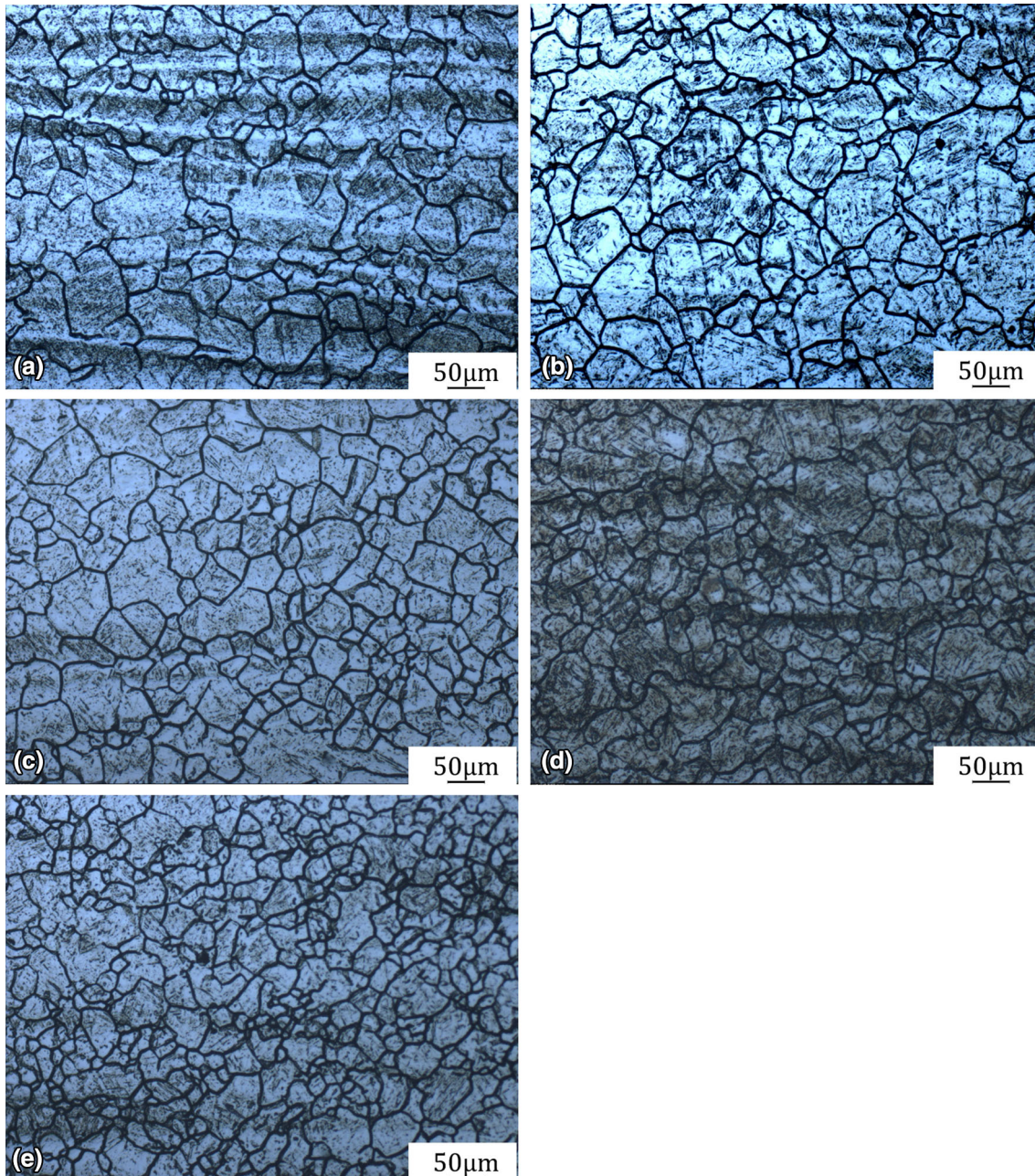
Fig. 3 Optical microstructures of samples deformed at different strain rates ($t = 1020$ °C, $\varepsilon = 0.912$): (a) 0.05 s^{-1}; (b) 0.1 s^{-1}; (c) 0.5 s^{-1}; (d) 1 s^{-1}; and (e) 3 s^{-1}

hardening is dominant and DRX has not yet been initiated. The dislocation density and distortion energy increase with increase in deformation strain, and DRX commences. The degree of DRX and grain refinement is enhanced with an increase in deformation capacity. When the deformation strain exceeds the peak strain, stress softening becomes dominant. During steady deformation, with an increase in strain, dynamic equilibrium is reached between work hardening and stress softening, and the DRX fraction will be close to constant.

3.4 Effect of Initial Austenite Grain Size

Figure 6 shows optical microstructures of the LZ50 steel with different austenite grain sizes D_0, for a total strain of 0.912, strain rate of 0.5 s^{-1}, and deformation temperature of

950 °C. When the D_0 values were 43.45, 64.81, 84.35, and 228.14 μm, the DRX grain sizes were 31.46, 24.61, 29.43, and 42.82 μm, respectively. The DRX grain sizes changed slightly under the same deformation condition, despite the different initial austenite grain sizes. This result agrees well with the observations reported previously (Ref 15-17).

4. Discussion

4.1 Zener-Hollomon Parameter

DRX is thermally activated. In general, the Z parameter can be used to characterize the effect of deformation temperature
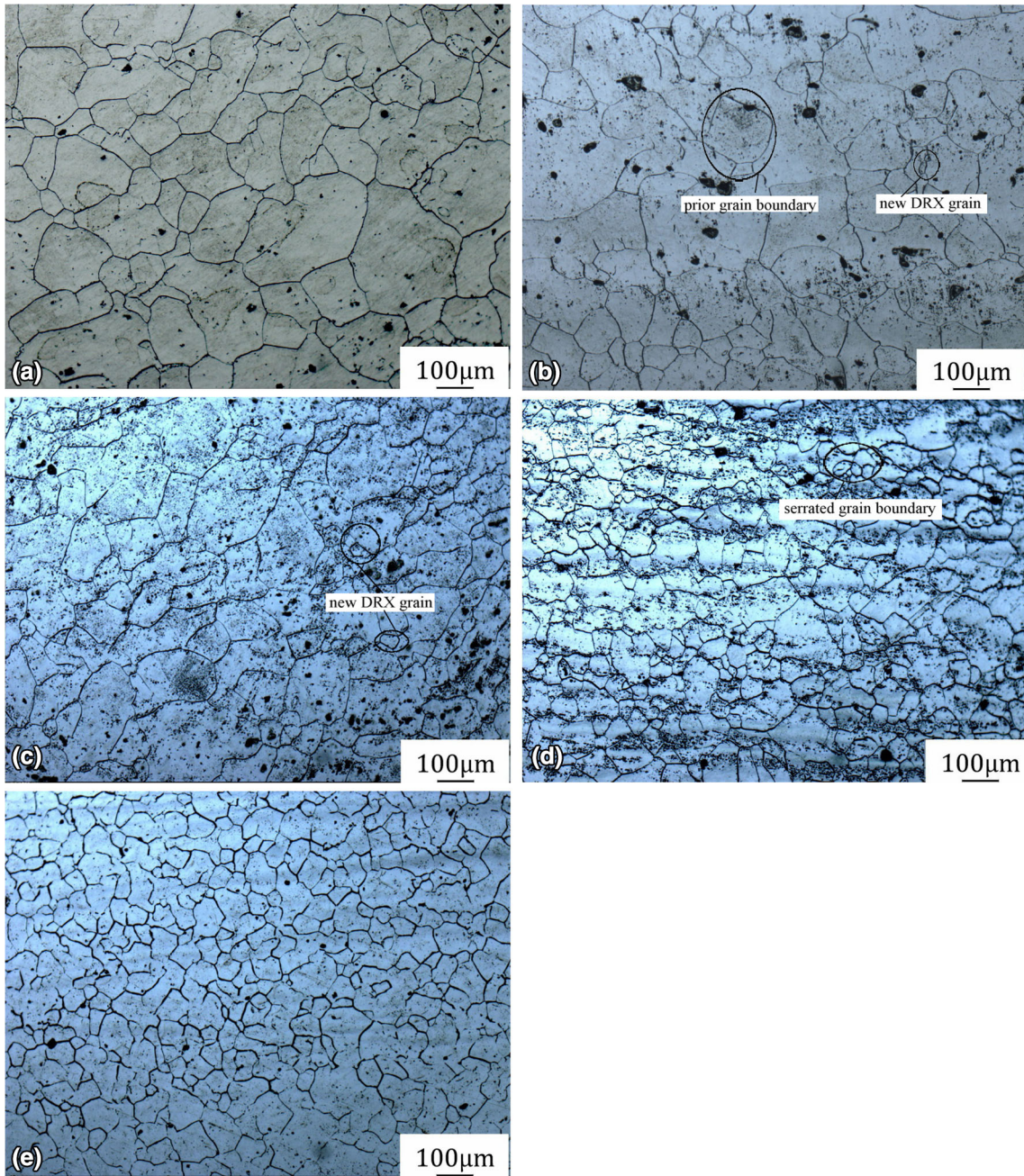
Fig. 4 Optical deformed microstructures under different strains ($t = 1070$ °C, $\dot{\varepsilon} = 0.5$ s^{-1}): (a) 0.163; (b) 0.223 (c) 0.288; (d) 0.511; and (e) 0.912

and strain rate on DRX behavior, and the relationship can be expressed as follows (Ref 18, 19):

$$Z = \dot{\varepsilon}\exp\left(\frac{Q}{RT}\right) = A[\sinh(\alpha\sigma_p)]^n, \quad \text{(Eq 1)}$$

where $\dot{\varepsilon}$ is the strain rate (s^{-1}); A, α, and n are constants that are independent of temperature; σ_p is the peak stress (MPa); Q is the hot deformation activation energy (J/mol); R is the gas constant; and T is the absolute temperature (K). For the selected steel, $\alpha = 0.01071$. n can be determined from the corresponding slopes of the fitting lines of $\ln\dot{\varepsilon} - \ln[\sinh(\alpha\sigma_p)]$. The average value of n can be estimated to be 4.4036. From the relationship curves of $\ln[\sinh(\alpha\sigma_p))$

and $10^3/T$, the average value of Q can be obtained as 304.27 kJ/mol. The activation energy of the experimental steel is very close to the Q value reported in previous research (Ref 6, 20, 21). The relationship curves of $\ln Z - \ln[\sinh(\alpha\sigma_p)]$ show that the average A can be obtained as 3.5884×10^{11}. By incorporating all the parameters into Eq 1, we obtain:

$$Z = \dot{\varepsilon}\exp\left(\frac{304270}{RT}\right) = 3.5884 \times 10^{11}[\sinh(0.01071\sigma_p)]^{4.4036}.$$

$$\text{(Eq 2)}$$

The work hardening rate θ ($\theta = d\sigma/d\varepsilon$), which is defined as the derivative of the true stress to true strain, reflects the relationship between the work hardening level and the true
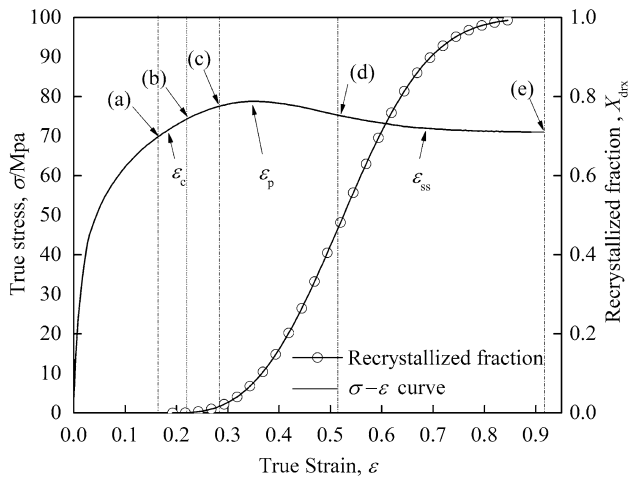
Fig. 5 Relationship between the flow stress, recrystallized fraction, and strain ($t = 1070$ °C, $\dot{\varepsilon} = 0.5$ s^{-1})

strain. Critical stresses for initiating DRX (σ_c) can be obtained from inflection points in the work hardening rate ($\theta = d\sigma/d\varepsilon$) versus flow stress ($\sigma$) curves or from the minima in the $-d\theta/d\sigma$ versus σ curves. Critical strains (ε_c) for the onset of DRX were obtained directly from the inflection points of the lnθ-ε curves. The relationship $\varepsilon_p = k'Z^p$ can be used to determine the relationship between ε_p and Z (Ref [22-24]), where k' and p are constants that are determined from the linear regression equation between lnε_p and ln$Z$. In previous reports, ε_c exists in a fixed proportion with ε_p. In this paper, the relationship between ε_c and ε_p obeys a linear equation and the following equations are obtained:

$$\varepsilon_p = 0.0013Z^{0.2105}, \qquad (Eq\ 3)$$

$$\varepsilon_c = 0.5146\varepsilon_p. \qquad (Eq\ 4)$$

4.2 DRX Kinetics

DRX is the main softening mechanism during hot deformation. In general, initially, the DRX rate is slow. Then, it increases rapidly with increasing strain until a considerable microstructure fraction is recrystallized. Finally, the DRX rate decreases again, and the DRX process is nearly complete. The form of the Avrami equation for DRX is (Ref [25])

$$X_{drx} = \frac{\sigma^A - \sigma}{\sigma_{s1} - \sigma_s} = 1 - \exp\left[-k\left(\frac{\varepsilon - \varepsilon_c}{\varepsilon_p}\right)^m\right], \qquad (Eq\ 5)$$

where X_{drx} is the volume fraction of DRX, σ^A is the flow stress when dynamic recovery is the only softening mechanism, σ_{s1} is the saturation stress, σ_s is the steady-state stress after DRX has progressed through the material, k and m are

constants, ε_c is the critical strain, and ε_p is the peak strain. All values were determined from the flow curve and by linear regression. The volume fraction model for DRX for the tested steel can be expressed as

$$X_{drx} = 1 - \exp\left(-0.8959\left(\frac{\varepsilon - \varepsilon_c}{\varepsilon_p}\right)^{2.9389}\right). \qquad (Eq\ 6)$$

The evolution of DRX microstructure grain size depends on the strain rate and deformation temperature and is independent of the initial grain size. The relationship between the average DRX grain size and the Z-parameter can be expressed by Eq [7], when DRX reaches a steady state (Ref [26]).

$$D_{drx} = CZ^{-k_1}, \qquad (Eq\ 7)$$

where D_{drx} is the austenite grain size after complete DRX (μm) and C and k_1 are the material constants. Through regression of the relationship between lnD_{drx} and ln$Z$, D_{drx} can be expressed as the power law function of the Z parameter as follows:

$$D_{drx} = 9.8738 \times 10^4 Z^{-0.2956}. \qquad (Eq\ 8)$$

Figure [7] compares the experimental and calculated DRX grain sizes. The calculated results agree with the experimental results, which confirms the accuracy of the proposed mathematical model. The mean error between the calculated and measured grain sizes is 5.6 μm.

4.3 Relationship Between DRX and Z Parameter

From an exact analysis of the flow curve, we can investigate the mechanism of hot working and minimize the microstructural examination. Based on this analysis and combined with the microstructural observations, different features of a deformed and recrystallized microstructure can be predicted and are summarized in the DRX map in Fig. [8]. First, critical strains for the onset of DRX (ε_c) are found directly from the inflection points of the lnθ-ε curves as shown in Fig. [9](a). The steady-state strain is obtained from Fig. [9](b). Certain values for ln$Z$, X_{drx}, ε_c, and ε_{ss} at different deformation conditions are shown in Table [2]. For a certain Z, we can plot ε_c and ε_{ss} in Fig. [8]. Then, the curve is fitted for ε_c and ε_{ss}. The upper limit (full DRX microstructure structure) in this map is the steady-state strain (ε_{ss}). However, the lower limit of this map is the critical strain for the initiation of DRX (ε_c). The DRX map can be used to predict features of a deformed and recrystallized microstructure.

In this map, a critical value of Z_c is identified above which the initiation of DRX is impossible. As the initial microstructure has a pronounced effect on DRX kinetics and critical strain, Z_c is related to the initial grain size and strain. In this case, the critical Z_c was $\sim 2.255 \times 10^{14}$, where the initial grain size was 342.84 μm.

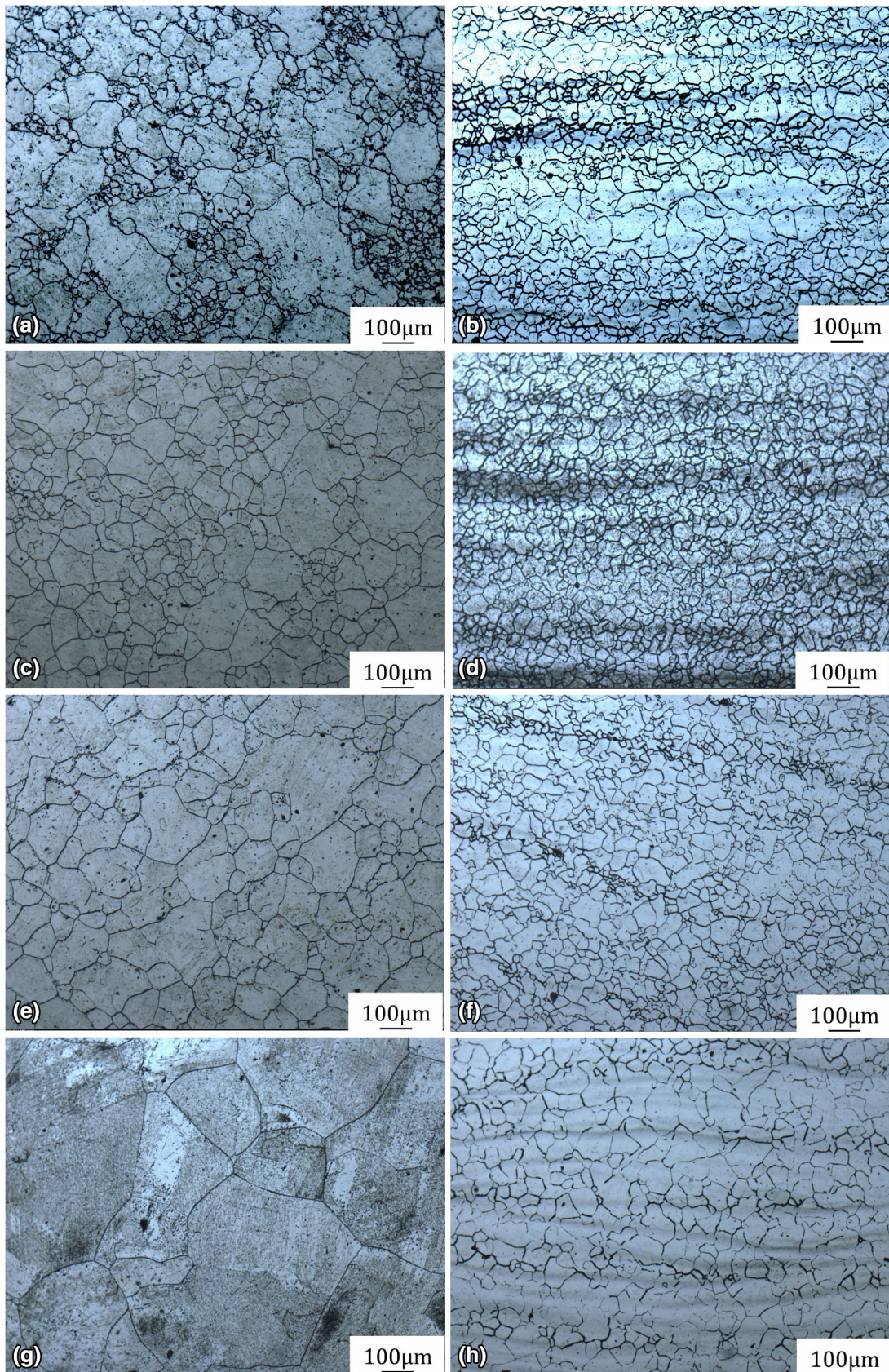**Fig. 6** Optical deformed microstructures with different initial austenite grain sizes ($t = 950$ °C, $\varepsilon = 0.912$, $\dot{\varepsilon} = 0.5$ s^{-1}): (a) 970 °C before deformation; (b) 970 °C after deformation; (c) 1020 °C before deformation; (d) 1020 °C after deformation; (e) 1070 °C before deformation; (f) 1070 °C after deformation; (g) 1170 °C before deformation; and (h) 1170 °C after deformation
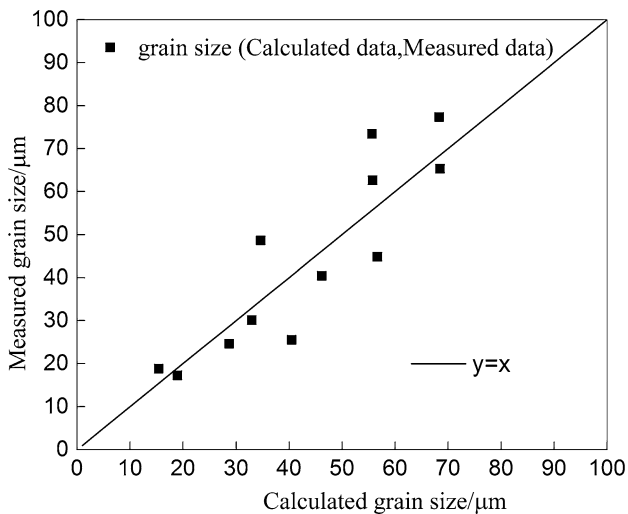
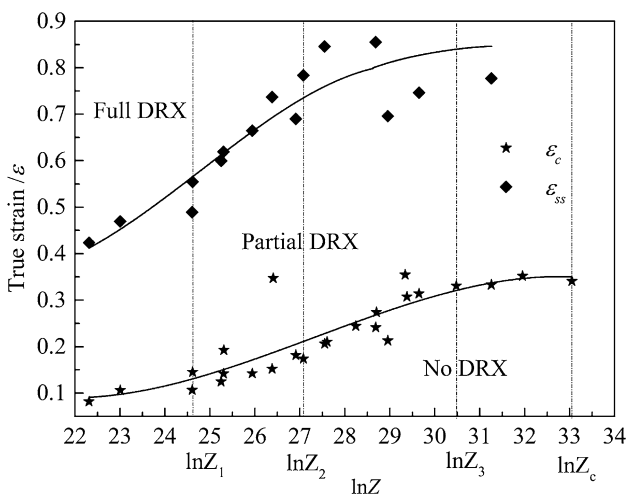**Fig. 7** Comparison between the calculated and measured values of the recrystallized grain size

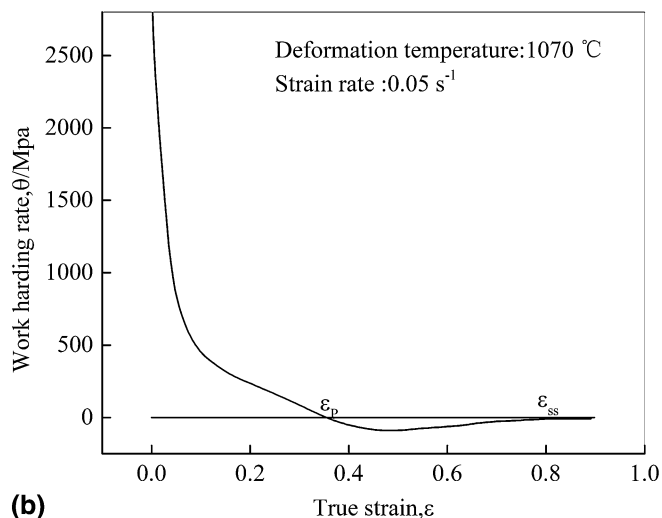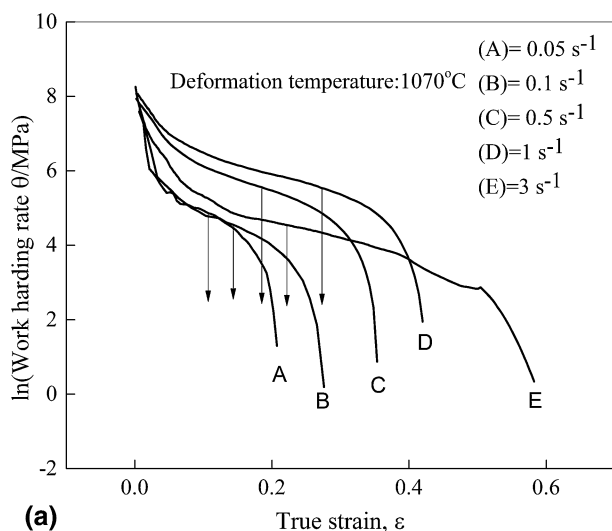**Fig. 8** DRX map of the LZ50 steel at a constant initial grain size of 342.84μm

Fig. 9 Relationship between (a) lnθ and ε and (b) θ and ε at 1070 °C

The relationship between DRX microstructure (grain size and recrystallization fraction) and Z parameter is shown in Fig. 10. Five regions are divided according to the DRX microstructure and Z parameter. For $Z < Z_1$ ($Z_1 = 4.865 \times 10^{14}$), the DRX fraction is 1, which means that DRX is completed. The grain size increases rapidly with decrease in Z. Grain coarsening occurred. In this area, the grain size slope decreases significantly. For $Z_1 < Z < Z_2$ ($Z_2 = 4.865 \times 10^{11}$), full DRX is completed and the DRX fraction is 1. The mean grain size decreases with increase in Z. This means that when the LZ50 steel process parameter is within this region, full DRX occurs and a fine recrystallization microstructure is obtained. For $Z_2 < Z < Z_3$ ($Z_3 = 1.725 \times 10^{13}$), the DRX fraction decreases with increase in Z, and the mean grain size changes slightly. A fine grain size may also be obtained. For $Z_3 < Z < Z_c$, with an increase in Z, the DRX fraction is close to 0, and the DRX is not obvious. The mean grain size is almost the same. With increase in Z, the DRX fraction is close to 0, and DRX is not obvious. The slope of the grain size remains almost constant. An analysis of the microstructure under the corresponding deformation conditions shows mixed crystals, which do not improve the material properties.

The general descriptive model for DRX is that nucleation occurs at serrated pre-existing grain boundaries and increases until a layer of DRX grains covers these boundaries (Ref 5). Then the recrystallization reaction proceeds until new grains consume the structure. This type of DRX structure is termed a necklace structure.

While Z is low, DRX kinetics are high. The critical strain is lower, which means that DRX grain nucleation starts at a very low strain. Under this condition, grain boundary mobility is very high, and new grains separate from the pre-existing grain boundary and grow very rapidly. As a result, a large number of serrated boundaries cannot be maintained for an extended period. At low Z values, the bulging mechanism is important. A large number of new grains appear, which prevents the formation of a necklace structure. For low Z values, the formation of a necklace structure is less than that for moderate Z conditions.

Compared with moderate or high Z values, the grain size for low Z conditions was non-homogeneous and some large grains were visible, as shown in Fig. 1(e). For a low Z, work hardening does not

Table 2 Values of $\ln Z$, X_{drx}, ε_c, and ε_{ss} at different deformation conditions

| Deformation temperature, °C	Strain rate, s^{-1}	$\ln Z$	X_{drx}	Critical strain ε_c	Steady-state strain ε_{ss}
1170	0.05	22.31246	1	0.0819	0.4236
1170	0.1	23.00561	1	0.1061	0.4695
1070	0.05	24.60799	1	0.1067	0.4893
1170	0.5	24.61504	1	0.1452	0.5546
1020	0.05	25.24845	1	0.1248	0.5997
1070	0.1	25.30113	1	0.1419	0.6192
1020	0.1	25.94159	1	0.1424	0.6646
970	0.05	26.38457	1	0.1521	0.7368
1070	0.5	26.91057	1	0.1817	0.69
970	0.1	27.07772	0.982	0.1739	0.7837
1020	0.5	27.55103	0.956	0.2063	0.8456
970	0.5	28.68716	0.634	0.2413	0.8552
870	0.05	28.95503	0.540	0.2128	0.696
870	0.1	29.64817	0.323	0.3139	0.7464
870	0.5	31.25761	0.054	0.333	0.7771
870	1	31.95076	0.018	0.3521	…
870	3	33.04937	0.001	0.3409	…
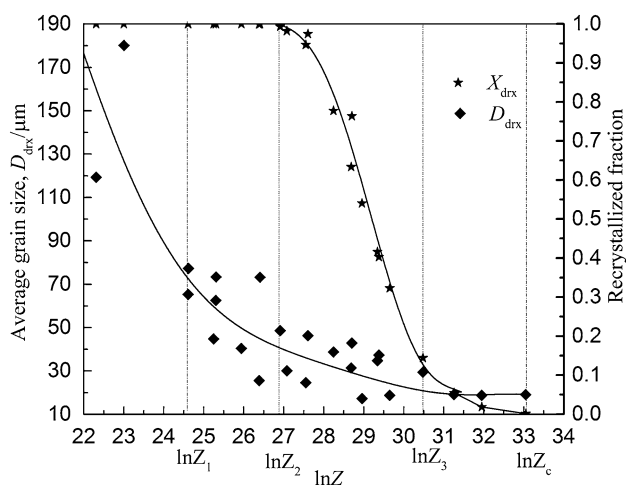
Fig. 10 Relationship between the DRX microstructure and Z

prevent recrystallized grain growth as for a high or moderate Z and the recrystallized grains grow rapidly. Therefore, some DRX grains that formed early grow rapidly and prevent adjacent grain growth. For high Z values, the critical strain will be high, and DRX initiation will be delayed, which results in a high level of work hardening. When DRX is initiated, a large number of new DRX grains will nucleate. The high fraction of new grains grows simultaneously, and these grains could not grow to a large size because of impingement.

In conclusion, for LZ50 steel, the hot deformation condition will be $Z_1 < Z < Z_3$, to achieve a fine grain size and to improve the mechanical properties. Figure 9 shows that while Z varies from Z_1 to Z_3, the DRX grain size decreases with increase in Z. To obtain a fine DRX grain structure, a high Z value should be chosen for $Z_1 < Z < Z_3$.

5. Conclusions

Hot compression tests for LZ50 steel were conducted from 870 to 1170 °C and for a strain rate from 0.05 to 3 s^{-1}. The effects of different deformation parameters such as temperature,

strain, and strain rate were investigated. The most important results are as follows:

(1) The effect of deformation temperature, strain, strain rate, and initial grain size on DRX behavior and microstructure evolution was analyzed. The Z parameter was analyzed by hyperbolic sine function. A model based on the Avrami equation was developed to estimate the DRX kinetics.

(2) The complete DRX grain size was independent of initial grain size and decreased with increasing strain rate and decreasing temperature under steady-state conditions. A mathematical equation of DRX grain size for LZ50 steel was proposed.

(3) A DRX map, which will provide guidelines for selecting suitable deformation parameters, was developed to show the different recrystallized microstructures as a function of Z. The onset of DRX was when the Zener-Hollomon parameter was less than the critical value Z_c, and the strain was higher than the critical strain ε_c. Hot deformation conditions were proposed to obtain a fine grain size in LZ50 steel and to improve the steel mechanical properties.

References

1. N.D. Ryan and H.J. McQueen, Flow Stress, Dynamic Restoration, Strain Hardening and Ductility in Hot Working of 316 Steel, *J. Mater. Process. Techol.*, 1990, **21**(2), p 177–199
2. A. Dehghan-Mashadi and P.D. Hodgson, Effect of δ-Ferrite Co-existence on Hot Deformation and Recrystallization of Austenite, *J. Mater. Sci.*, 2008, **43**(18), p 6272–6277

3. A. Momeni and K. Dehghani, Prediction of Dynamic Recrystallization Kinetics and Grain Size for 410 Martensitic Stainless Steel During Hot Deformation, *Met. Mater. Int.*, 2010, **16**(5), p 843–849

4. S.D. Gu, L.W. Zhang, J.H. Ruan, P.Z. Zhou, and Y. Zhen, Constitutive Modeling of Dynamic Recrystallization Behavior and Processing Map of 38MnVS6 Non-quenched Steel, *J. Mater. Eng. Perform.*, 2014, **23**(3), p 1062–1068

5. A. Dehghan-manshadi, M.R. Barnett, and P.D. Hodgson, Hot Deformation and Recrystallization of Austenitic Steel, Part I. Dynamic Recrystallization, *Metall. Mater. Trans. A*, 2008, **39A**(6), p 1359–1370

6. S.L. Zhu, H.Z. Cao, J.S. Ye, W.H. Hu, and G.Q. Zheng, Dynamic Recrystallization Behavior of Medium Carbon Cr-Ni-Mo-Nb Steel During Hot Deformation, *J. Iron Steel Res. Int.*, 2015, **22**(3), p 264–271

7. A. Momeni, S.M. Abbasi, and A. Shokuhfar, Hot Compression Behavior of As-Cast Precipitation-Hardening Stainless Steel, *J. Iron Steel. Res. Int.*, 2007, **14**(5), p 66–70

8. S.M. Abbasi and A. Shokuhfar, Prediction of Hot Deformation Behaviour of 10Cr–10Ni–5Mo–2Cu Steel, *Mater. Lett.*, 2007, **61**(11–12), p 2523–2526

9. R. Ebrahimi, S.H. Zahiri, and A. Najafizadeh, Mathematical Modelling of the Stress-Strain Curves of Ti-IF Steel at High Temperature, *J. Mater. Process. Technol.*, 2006, **171**(2), p 301–305

10. A. Belyakov, H. Miura, and T. Sakai, Dynamic Recrystallization in Ultra Fine-Grained 304 Stainless Steel, *Scr. Mater.*, 2000, **43**(1), p 21–26

11. T. Sakai and J.J. Jonas, Overview No. 35 Dynamic Recrystallization: Mechanical and Microstructural Considerations, *Acta Metall.*, 1984, **32**(2), p 189–209

12. M. Ueki, S. Horie, and T. Nakamura, Factors Affecting Dynamic Recrystallization of Metals and Alloys, *Mater. Sci. Technol.*, 1987, **3**(5), p 329–337

13. K.W. Kim and J.K. Park, A Study of the Dynamic Recrystallization Kinetics of V-Microalloyed Medium Carbon Steel, *J. Mater. Sci.*, 2015, **50**(18), p 6142–6153

14. B. Derby and M.F. Ashby, On Dynamic Recrystallization, *Scr. Metall.*, 1987, **21**, p 879–884

15. B.X. Wang, X.H. Liu, and G.D. Wang, Dynamic Recrystallization Behavior and Microstructure: Evolution in Mn-Cr Gear Steel, *Mater. Sci. Eng. A*, 2005, **393**(1–2), p 102–108

16. L.Z. Wu, X.S. Li, J. Chen, H.B. Zhang, and Z.S. Cui, Dynamic Recrystallization Behavior and Microstructure Evolution in SPHC Steel, *J. Shanghai Jiaotong Univ. (Sci.)*, 2010, **15**(3), p 301–306

17. F. Montheillet, O. Lurdos, and G. Damamme, A Grain Scale Approach for Modeling Steady-State Discontinuous Dynamic Recrystallization, *Acta Mater.*, 2009, **57**(5), p 1602–1612

18. H. Mirzadeh, Quantification of the Strengthening Effect of Reinforcements During Hot Deformation of Aluminum-Based Composites, *Mater. Des.*, 2015, **65**, p 80–82

19. H. Mirzadeh, Constitutive Modeling and Prediction of Hot Deformation Flow Stress Under Dynamic Recrystallization Conditions, *Mech. Mater.*, 2015, **85**, p 66–79

20. S. Saadatkia, H. Mirzadeh, and J.M. Cabrera, Hot Deformation Behavior, Dynamic Recrystallization, and Physically-Based Constitutive Modeling of Plain Carbon Steels, *Mater. Sci. Eng. A*, 2015, **636**, p 196–202

21. L.Y. Lan, C.L. Qiu, D.W. Zhao, X.H. Gao, and L.X. Du, Dynamic and Static Recrystallization Behavior of Low Carbon High Niobium Microalloyed Steel, *J. Iron. Steel. Res. Int.*, 2011, **18**(1), p 55–60

22. L. Deng, X.Y. Wang, J.C. Xia, and H.T. Guo, Microstructural Modeling and Simulation of Al-2.8Cu-1.4Li Alloy During Elevated Temperature Deformation, *Metall. Mater. Trans. A*, 2011, **42A**(8), p 2509–2515

23. C.M. Sellars and J.A. Whiteman, Recrystallization and Grain Growth in Hot Rolling, *Met. Sci.*, 1979, **13**(3–4), p 187–194

24. F. Yin, L. Hua, H.J. Mao, X.H. Han, D.S. Qian, and R. Zhang, Microstructural Modeling and Simulation for GCr15 Steel During Elevated Temperature Deformation, *Mater. Des.*, 2014, **55**, p 560–573

25. Y.G. Liu, M.Q. Li, and J. Luo, The Modelling of Dynamic Recrystallization in the Isothermal Compression of 300M Steel, *Mater. Sci. Eng. A*, 2013, **574**, p 1–8

26. F. Chen, Z.S. Cui, and S.J. Chen, Recrystallization of 30Cr2Ni4MoV Ultra-Super-Critical Rotor Steel During Hot Deformation, Part I: Dynamic Recrystallization, *Mater. Sci. Eng. A*, 2011, **528**(15), p 5073–5080